Multi-Plateau Molecular High Harmonic Generation Frome Multi-Functional Group Recombination

Xinyue Xie(谢欣悦)[1], Guoxiang Luo(罗国相)[1*], and Xi Zhao(赵曦)[2*]

[1]*School of Physics and Electronics, Qiannan Normal University for Nationalities, Duyun 558000, China*
[2]*School of Physics and Information Technology, Shaanxi Normal University, Xi'an 710062, China*

(Received 16 May 2025; accepted manuscript online 11 August 2025)

Permanent dipole moments induced high-order harmonic generation (HHG) signals offer a potential approach to producing elliptically or even circularly polarized X-ray attosecond sources. Previous studies on this topic have mainly focused on diatomic molecules such as CO and HeH. Based on this scheme, significant HHG signals in the direction perpendicular to the molecular axis can be observed in both the high-energy and low-energy regions. However, we found that the high-order harmonics induced by the permanent dipole moments of polyatomic complex molecules involve more intricate physical processes. Using time-dependent density functional theory, we simulated the dynamics of HHG from NH_2COOH and NH_2COSH interacting with linearly polarized lasers. We found that the harmonic signals in the direction perpendicular to the N-C bond were significantly enhanced in the high-energy photon region. Our analysis indicates that this is due to the complex molecular configuration of NH_2COOH and NH_2COSH: while the NH_2 group has C_{2v} symmetry, both COOH and COSH groups lack this symmetry. This structural characteristic results in permanent dipole moments being felt only when electrons return to either COSH or COOH groups, but not to NH_2 group. Additionally, our results reveal a multi-plateau structure in HHG signal along laser polarization direction, a phenomenon arising from multi-electron and multi-orbital effects during interaction between complex molecule and strong laser field.

DOI: 10.1088/0256-307X/42/10/100301 CSTR: 32039.14.0256-307X.42.10.100301

High-order harmonic generation (HHG) is a nonlinear optical process where a target, typically an atom or molecule, is exposed to an intense laser field, resulting in the emission of photons with energies that are multiples of the original photon energy.[1–8] This process has become an invaluable tool in time-resolved spectroscopy,[9–17] molecular orbital imaging,[18–22] and the synthesis of extreme ultraviolet pulses.[23–28] Characterized by its capability to attain attosecond time resolution, HHG has become a versatile and indispensable tool in modern spectroscopy, paving the way for new discoveries in physics, chemistry, and material science.

Specifically, the permanent dipole moment in molecular systems plays a crucial role in HHG by breaking the inversion symmetry of the system, which allows for the generation of even harmonics in addition to the typical odd harmonics.[29–33] This results in richer spectral features and provides insights into the asymmetric charge distribution and molecular structure. The dipole interacts strongly with the laser field, affecting electron dynamics and leading to asymmetric emission profiles that depend on the molecule's orientation relative to the field. This makes HHG a powerful tool for probing molecular structures, ultrafast charge dynamics, and molecular imaging, offering access to information that is otherwise inaccessible in centrosymmetric systems. In recent years, theoretical studies on the effects of permanent dipole moments on HHG have primarily focused on diatomic molecules[34–41] such as CO and HeH. Hu *et al.* discovered that when a linearly polarized laser is applied parallel to the molecular axis of a CO molecule, pure even-order harmonics from order 10 (H10) to order 50 (H50) can be observed in the direction perpendicular to the molecular axis.[42]

However, studies on the effects of permanent dipole moments on the HHG dynamics of polyatomic molecules remain relatively scarce. In this work, we used real-time, real-space, and time-dependent density functional theory (TDDFT) to study the HHG emission in the perpendicular direction induced by permanent dipole moments in complex polyatomic molecules NH_2COOH and NH_2COSH. Unlike the results of Hu *et al.*, we found that harmonic signals in the direction perpendicular to the N-C molecular axis are enhanced in the high-energy photon region.

Further analysis revealed that this phenomenon arises from the complex structure of NH_2COOH and NH_2COSH. The selected molecules consist of two groups: an NH_2 group and a COSH (or COOH) group. These two groups have different symmetries: the NH_2 group has C_{2v} symmetry, while the COSH (or COOH) group does not exhibit C_{2v} symmetric structure. In other words, for NH_2COSH (or NH_2COOH) molecules, their permanent dipole moments originate only from the COSH (or COOH) group. When the ionized electron returns to the NH_2 group, it does not experience the influence of the permanent dipole

*Corresponding authors. Email: luoguoxiang2008@yeah.net; zhaoxi719@snnu.edu.cn
© 2025 Chinese Physical Society and IOP Publishing Ltd. All rights, including for text and data mining, AI training, and similar technologies, are reserved.

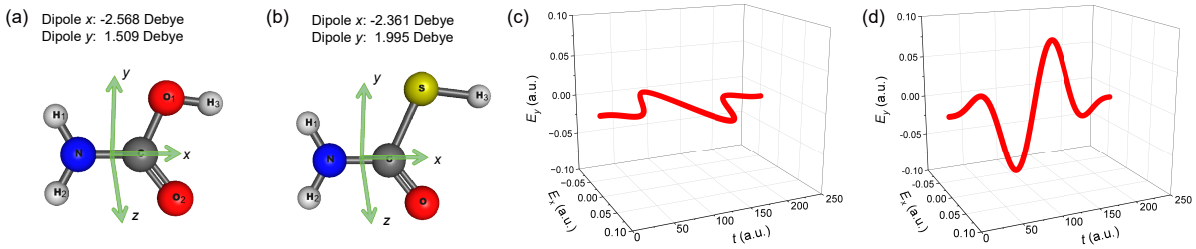

Fig. 1. (a) Geometry and dipole moment of NH_2COOH (carbamic acid). (b) Geometry and dipole moment of NH_2COSH (carbamothioic S-acid). (c) Electric field of x-direction $I = 2.84 \times 10^{14}\,\mathrm{W/cm^2}$, $\lambda = 800\,\mathrm{nm}$, $\varphi = 0$. (d) Electric field of y-direction $I = 2.84 \times 10^{14}\,\mathrm{W/cm^2}$, $\lambda = 800\,\mathrm{nm}$, $\varphi = 0$.

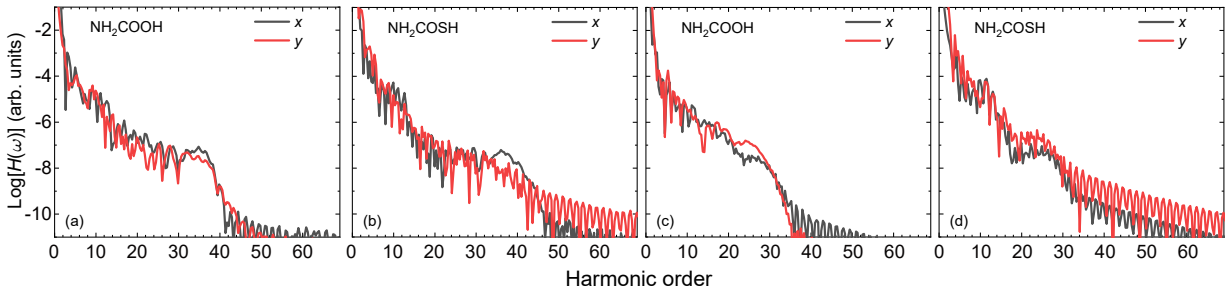

Fig. 2. Higher-order harmonic spectra of NH_2COOH and NH_2COSH molecules. (a) and (b) The laser is polarized in the x-direction. (c) and (d) The laser is polarized in the y-direction.

moments. However, it does feel the effect of the permanent dipole moments when returning to the COSH (or COOH) group.

Our results demonstrate that the microscopic spatial structure of molecules has a crucial impact on laser-induced nonlinear optical processes. On the other hand, this influence can be utilized to trace and control the ultrafast dynamics of electrons in complex systems.

The main results of our work were obtained using the TDDFT software package `octopus`.[43–45] Details of our computational methods can be found in the Supplementary Materials (SM). For the theoretical background of TDDFT, please refer to Refs. [46–48] and some references therein. Atomic units are used in this article unless otherwise stated.

We first investigated the high-order harmonic properties of NH_2COSH (carbamothioic S-acid) and NH_2COOH (carbamic acid) molecules using linearly polarized lasers aligned along the x- and y-axes, respectively. Figures 1(a) and 1(b) illustrate the molecular structures and dipole moments of NH_2COSH and NH_2COOH in Cartesian coordinates, with the N-C bond oriented along the x-axis. From a molecular configuration perspective, the NH_2 group exhibits C_{2v} symmetry, while the COOH and COSH groups do not possess this symmetry. We label the H atoms as H_1 and H_2 on the NH_2 group (H_1 above and H_2 below) and as H_3 on the COOH and COSH groups. The O atoms in the COOH group are designated as O_1 (above) and O_2 (below). The polarization directions of the laser pulses are indicated along the x- and y-axes, as shown in Figs. 1(c) and 1(d).

Figure 2 presents the high-order harmonic spectra of the two molecules under different laser polarization directions. Figures 2(a) and 2(b) show the harmonic spectra for laser polarization along the x-axis, while Figs. 2(c) and 2(d) correspond to polarization along the y-axis. In these plots, the black lines represent the high-order harmonics emitted along the x-axis, while the red lines correspond to those emitted along the y-axis. The results reveal that the HHG signal perpendicular to the polarization direction enhanced in the high-energy region. To investigate the origin of this harmonic behavior, we focus on the NH_2COSH molecule, which has the most complex configuration among the studied cases.

We present our main results in Fig. 3. The electric field, with an intensity of $I = 2.84 \times 10^{14}\,\mathrm{W/cm^2}$ and a two cycle duration, is polarized along the x-axis. Driven by this field, the corresponding HHG spectra are given in Figs. 3(a) and 3(b), and the time-frequency analysis plots are shown in Figs. 3(c) and 3(d).

At first glance, we observe that the HHG in the x-direction exhibits two plateaus, while the HHG in the y-direction exhibits one plateau. The temporal-frequency analysis for HHG in the x- and y- directions are presented in Figs. 3(c) and 3(d), respectively. These results indicate three instances of high-energy photon emission in the HHG process:

(i) The first emission occurs between $t = 110$ and $t = 160$, producing the first plateau (H8 to H13) in the x-direction.

(ii) The second emission occurs between $t = 135$ and $t = 170$, resulting in the second plateau (H23 to H36) in the x-direction.

(iii) The third emission occurs between $t = 160$ and $t = 175$, generating the plateau in the y-direction with similar photon energy to the second plateau.

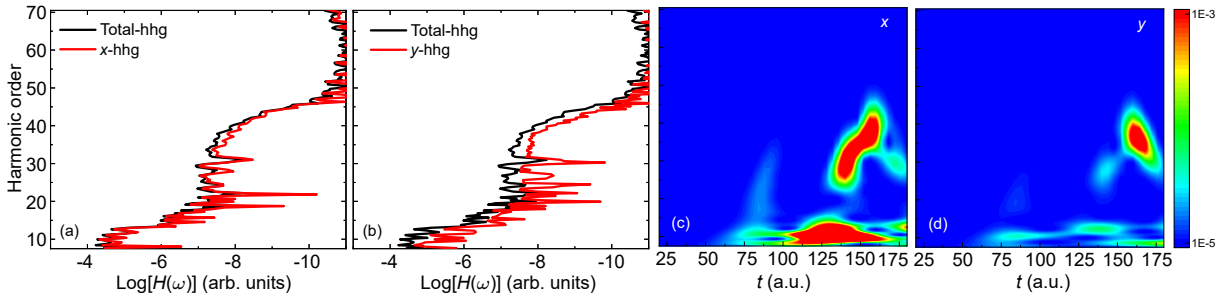

Fig. 3. (a) The HHG spectra of NH_2COSH, total (black solid line) and x-direction (red dashed line). (b) The HHG spectra of NH_2COSH, total (black solid line) and y-direction (red dashed line). (c) Time-frequency behavior of x-direction. (d) Time-frequency behavior of y-direction.

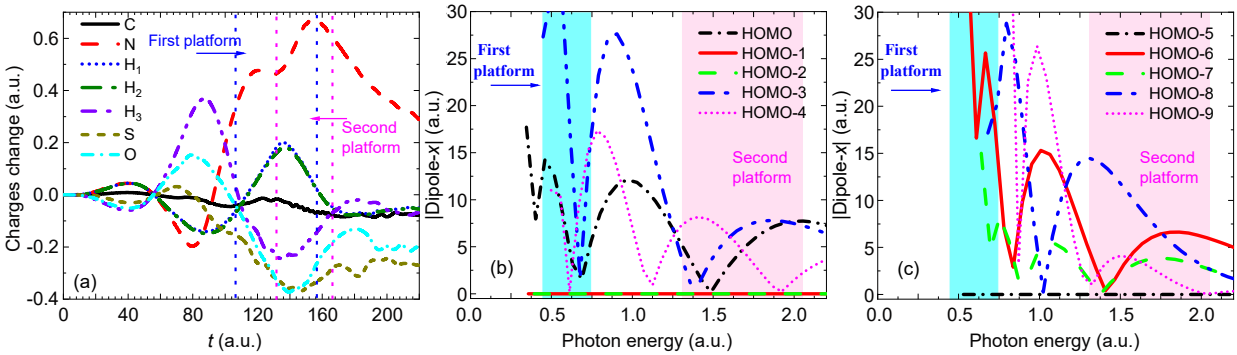

Fig. 4. (a) The change in the amount of charge around each nucleus over time. (b) and (c) Modulus of dipole in the different molecular orbitals calculated using plane-wave approximation in the x-direction.

Notably, the third emission follows the second emission very closely in time. Next, we analyze our results using both the classical three-step model and the perspective of light-induced quantum transitions. The classical three-step model focuses on the electron dynamics under the influence of a strong laser field, while the quantum transition calculation emphasizes the ionization-recombination pathways of the electrons.

In atomic or simple molecular systems, the HHG dynamics can be well described by the so-called three-step model: a strong laser field ionizes an atom or molecule, freeing an electron; then the oscillating electric field of the laser accelerates the free electron; finally, the electron recombines with the parent ion, releasing high-energy photons. This model explains the generation of HHG, characterized by a plateau in the spectrum followed by a sharp cutoff. The highest energy photons are determined by the ionization potential and the kinetic energy gained by the electron during acceleration. The three-step model is crucial for understanding ultrafast nonlinear dynamics and has advanced the field of attosecond science. In our calculations, although the electron can move in three-dimensional space, it only experiences the force of the electric field in the x-direction. Therefore, our classical trajectory calculations consider only the x-direction.

However, in more complex molecules, some ionized electrons may not return to their original nucleus when they revert to the parent ion. To identify which nucleus the HHG signals originate from, we calculated the charge distribution changes near each nucleus [as shown in Fig. 4(a)]. The transition dipole moments (TDM) from HOMO to HOMO-9 in the x-direction are provided in Figs. 4(b) and 4(c). We also calculated the orbital energies in Table 1 and the classical kinetic energies of the electron as a function of electron returning time, as shown in Fig. 5. "A-B" in the figures corresponds to the electron ionizing from atom A and returning at atom B, "RC" indicates that electrons ionized from atom A recombine back with atom A itself. In our revisited three-step model calculating the kinetic energy of returning electrons, only the x-direction distance between atoms is considered. In the NH_2COSH molecule, the x-axis positions of the S and O atoms are identical, as are those of H_1 and H_2 atoms; we will address this assumption later.

Table 1. KS orbital energy (E_{ks}) calculated by DFT.

Orbital	Energy	Orbital	Energy
HOMO	−0.345298	HOMO-6	−0.552612
HOMO-1	−0.356744	HOMO-7	−0.640359
HOMO-2	−0.39315	HOMO-8	−0.681088
HOMO-3	−0.448809	HOMO-9	−0.814187
HOMO-4	−0.497966	HOMO-10	−0.963709
HOMO-5	−0.529786	HOMO-11	−1.071516

The above data draw a clear pattern of HHG dynamics. The first plateau's emission occurs between $t = 110$ and $t = 160$, and the energies ranging from 0.456 to 0.741. In this time range, the charge around the NH_2 group increases [see Fig. 4(a), the red, blue and green dashed lines], suggesting that the first plateau HHG primarily originates from electrons returning to the NH_2 group. In this energy range, the TDM of the HOMO-3 and HOMO-6 orbitals

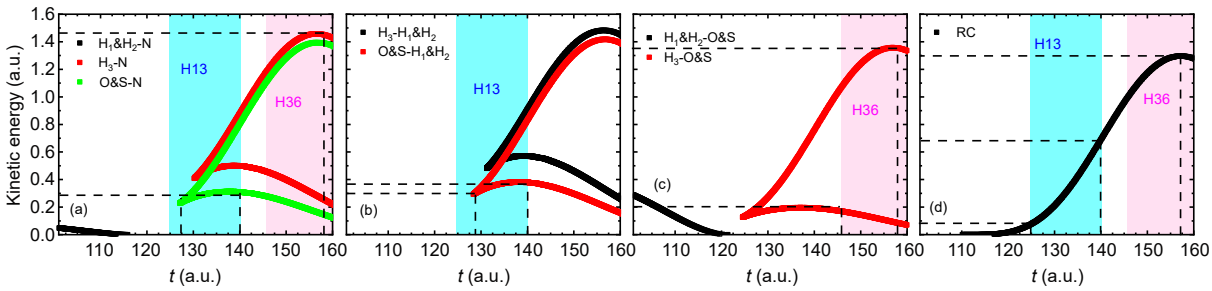

Fig. 5. The return kinetic energy of the electron as a function of the recombination time. (a) Electrons ionized from H_1 or H_2 (black dots), from H_3 (red dots), from O or S (green dots) back to the N atom. (b) Electrons ionized from H_3 (black dots), from O or S (red dots) back to the H_1 or H_2 atom. (c) Electrons ionized from H_1 or H_2 (black dots), from H_3 (red dots) back to the O or S atom. (d) The ionized electron returns to its original nucleus.

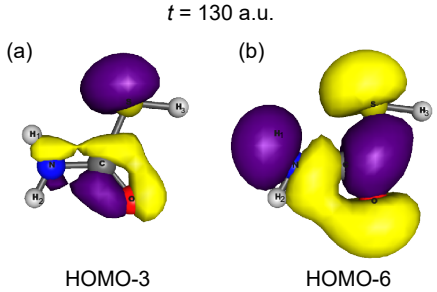

Fig. 6. Molecular orbitals diagram at $t = 130$ a.u. for (a) HOMO-3 (b) HOMO-6.

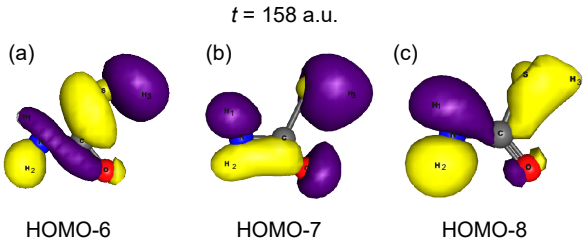

Fig. 7. Molecular orbitals diagram at $t = 158$ a.u. (a) HOMO-6. (b) HOMO-7. (c) HOMO-8.

are considerably large [see Figs. 4(b) and 4(c)], indicating that these orbitals may contribute to the first plateau HHG. Following this, we conduct a quantitative analysis using H13 as an example, which is emitted between $t = 125$ and $t = 140$. According to Table 1, the orbital energy of HOMO-3 differs by 0.3 from the H13, aligning with the kinetic energy for electrons traveling from the O or S atom to the NH_2 group [see the green line in Fig. 5(a) and the red line in Fig. 5(b)]. The orbital energy of HOMO-6 differs by approximately 0.2 from the H13, correlating with the kinetic energy of the RC mechanism [see Fig. 5(d), black line].

Noting that our three-step model cannot identify whether electrons return to the H_1 or H_2 atom, we calculate the orbital wave function at the time of electron return ($t = 130$) as shown in Fig. 6. This approach provides insight into the specific nucleus to which the electron returns in this molecular system. Figure 6(a) illustrates that electrons ionized form COSH group predominantly recombine with the N or H_1 atom in the HOMO-3 orbital. Similarly, figure 6(b) demonstrates that free electrons originating from H_1 primarily return to the H_1 atom in the HOMO-6 orbital.

Next, we focus on the second plateau. The emission time of the second plateau is from $t = 135$ to $t = 170$, with energies ranging from 1.31 to 2.05. In this time range, the charge around the COSH group consistently increases [see Fig. 4(a), the light blue, dark yellow, and purple dashed lines], while before $t = 160$, the charge around the N of atom increases [see Fig. 4(a), the red dashed line]. At a photon energy of approximately 2.052, HOMO-6, HOMO-7, and HOMO-8 orbitals are significantly large [see Fig. 4(c)]. Following this, we carry out a quantitative analysis using H36 as an example, emitted between $t = 146$ and $t = 160$. In Table 1, the orbital energies of HOMO-8, HOMO-7, and HOMO-6 differ from H36 by 1.37, 1.4, and 1.5, respectively. Meanwhile, from Fig. 5(a), it is evident that the kinetic energy of an electron returning to the N atom from either the O or S atoms is 1.4 (green line), and from H_3 atom it is 1.5 (red line). From Fig. 5(c), it shows that the kinetic energy from H_3 to O or S is also about 1.37 (red line).

To determine which atoms emits the harmonics, we investigate the molecular orbital function at $t = 158$ (shown in Fig. 7). Figures 7(a) and 7(b) illustrate that electrons ionized from the COSH group recombine with the N atom in the HOMO-6 and HOMO-7 orbitals. Figure 7(c) shows that electrons ionized by H_3 return to the S atom in the HOMO-8 orbital.

Finally, we switch our analysis to the y-direction HHG, which signal is enhanced in the high-energy region. As evident in Figs. 3(c) and 3(d), HHG in the y-direction follows the second harmonic platform emission in the x-direction ($t = 150$ to $t = 175$), and the energies range between 1.82 and 2.39. To reveal the contradiction of the y-direction HHG between Figs. 3(c) and 3(d), we decomposed the HHG dipole moments $d(t)$ into intrinsic $d_{\rm int}(t)$ and induced components $d_{\rm ind}(t)$. $d_{\rm int}(t)$ arises from the permanent dipole moments as studied in Ref. [42], while $d_{\rm ind}(t)$ originates from electron oscillation induced by the laser. The variation of dipole accelerations with time in the x-direction (black line) and the y-direction (red dashed line) is shown in Fig. 8(a), while the y-direction HHG of $d_{\rm int}(t)$ and $d_{\rm ind}(t)$ is illustrated in Fig. 8(b).

We can see in Fig. 8(a) that during this time range, the

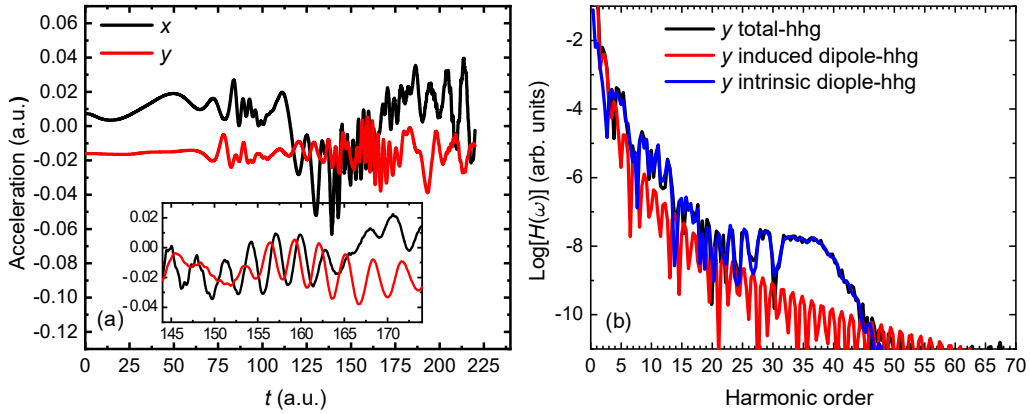

Fig. 8. (a) Variation of dipole acceleration with time, x-direction (black solid line), y-direction (red dashed line). (b) The HHG spectra of NH_2COSH in y-direction, total (black solid line), induced dipole (red dashed line), and electric dipole (blue dotted line).

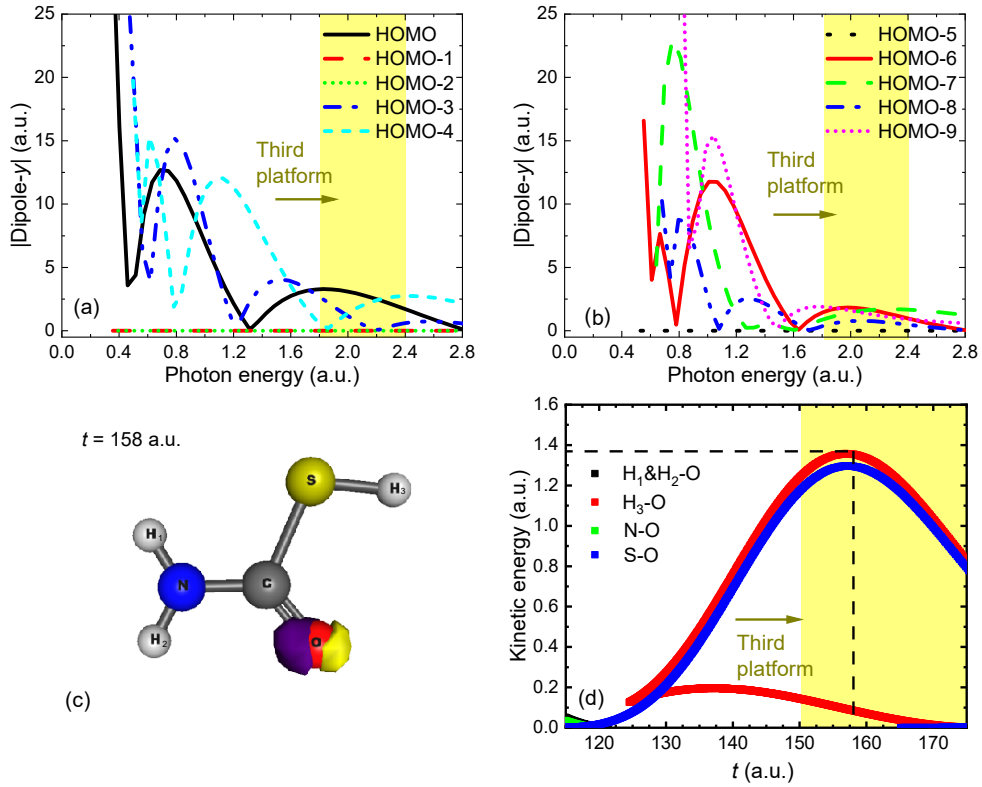

Fig. 9. (a) and (b) Modulus of dipole in the different molecular orbitals calculated using plane-wave approximation in the x-direction. (c) Diagram of current distribution at $t = 158$ a.u. (d) The return kinetic energy of the electron as a function of the recombination time, electrons ionized from H_1 or H_2 (black dots), from H_3 (red dots), from N (green dots), from S (blue dots) back to the O atom.

dipole acceleration on the y-axis closely follows the oscillation of the x-axis dipole acceleration, with a slight delay in the y-direction. These results indicate that HHG in the y-direction mainly comes from $d_{\text{int}}(t)$, which cannot be detected in temporal-frequency-analysis calculations, making the total y-direction HHG intensities comparable to those in the x-direction. This permanent dipole moment-induced HHG was first elucidated by Hu *et al.*[42]

In this energy range, the HOMO, HOMO-3, HOMO-4, HOMO-6, HOMO-7, HOMO-8, and HOMO-9 orbitals may contribute to the y-direction plateau [see Figs. 9(a) and 9(b)]. To determine which atom emits harmonics in the y-direction, we evaluated the current distribution at the juncture of harmonic emission, as depicted in Fig. 9(c). In particular, ionized electrons predominantly converge around the O atom along the y-direction.

Following this, we perform a quantitative analysis, taking H42 as an example. From Fig. 9(d), it is evident that the maximum kinetic energy in the x-direction is approximately 1.35, displaying a difference of around 1.04 compared to H42. Furthermore, the highest energy value of the contributory molecular orbitals indicated in Table 1

is −0.8817, illustrating that the source of this difference comes from the kinetic energy of the electrons in the y-direction.

Such y-direction $d_{\rm ind}(t)$ contributed HHG can be understood as follows: When the electrons are pulled back near the atom, there is a force from the permanent dipole moments, causing the electrons to turn and move in the y-direction and return to the O atom. This explains why the temporal-frequency analysis of the second plateau in the x-direction and that in the y-direction are so close in time. The origin of HHG in the y-direction, associated with the formation of the second plateau in the x-direction, can be deduced from Fig. 7. As shown in Fig. 7(a), the wave function is distributed along the y-axis between N and O atoms, indicating that under the influence of permanent dipole moments, electrons in HOMO-6 orbital, which are about to return to N atom, are deflected toward O atom. Similarly, figure 7(c) shows that electrons in HOMO-8 orbital attracted by S atom are also shifted towards O atom due to this influence. In contrast, figure 7(b) reveals a wave function aligned along x-axis between N and O atoms, which does not contribute to HHG in y-direction.

Based on the above analysis, the electron dynamics can be summarized in sequential phases: Initially, electrons near the O and S atoms shift rightward, then transition leftward. When the electric field reaches its reverse maximum, a portion of these electrons return to the N and H_1 atoms within the HOMO-3 orbital, initiating the first harmonic platform. Subsequently, more distant electrons return to the N atom in the HOMO-7 orbital, generating a second harmonic platform. Simultaneously, under the influence of the reversed electric field, electrons ionized from H_3 partially recombine at both the N atom of HOMO-6 orbital and S atom of HOMO-8 orbital, further contributing to the second harmonic platform. Subsequently, these electrons move in the y-direction under the influence of permanent dipole moments and eventually reach the vicinity of O atoms in that same orbital, forming a harmonic plateau in y-direction.

In summary, we theoretically investigated the HHG dynamics of the complex polyatomic molecules NH_2COSH and NH_2COOH. Our findings reveal that the HHG dynamics differs entirely depending on whether the returning electrons interact with one of the two molecular groups. The symmetric NH_2 group does not generate HHG signals perpendicular to the N-C bond, whereas electrons returning to the COSH or COOH groups produce high-energy photons in the perpendicular direction due to the influence of permanent dipole moments. Our study highlights that the internal structure of complex molecules plays a crucial role in the nonlinear electron dynamics induced by the laser field.

Acknowledgements. This work was supported by the Fundamental Research Funds for the Central Universities (Grant Nos. GK202207012 and QCYRCXM-2022-241).

References

[1] McPherson A, Gibson G, Jara H, Johann U, Luk T S, McIntyre I, Boyer K, and Rhodes C K 1987 *J. Opt. Soc. Am. B* **4** 595

[2] Lewenstein M, Balcou P, Ivanov M Y, L'huillier A, and Corkum P B 1994 *Phys. Rev. A* **49** 2117

[3] Qiao Y, Chen J Q, Zhou S S, Chen J G, Jiang S C, and Yang Y J 2024 *Chin. Phys. Lett.* **41** 014205

[4] Li Q Y, Li Y L, Guo F M, Yang Y J, Jin M X, Zhao X, and Wang J 2024 *Phys. Rev. A* **109** 063112

[5] Wang D, Zhu X, Liu X, Li L, Zhang X, Lan P, and Lu P 2017 *Opt. Express* **25** 23502

[6] Zhang C P and Miao X Y 2023 *Chin. Phys. Lett.* **40** 124201

[7] Chen J, Jiang W, Qiao Y, Yang Y, and Chen J 2025 *Chin. Phys. Lett.* **42** 013201

[8] Wang E, Wang Y, and Meng S 2025 *Chin. Phys. Lett.* **42** 047302

[9] Zhao X, Wang S J, Yu W W, Wei H, Wei C, Wang B, Chen J, and Lin C D 2020 *Phys. Rev. Applied* **13** 034043

[10] Le A T, Morishita T, Lucchese R, and Lin C D 2012 *Phys. Rev. Lett.* **109** 203004

[11] Borrego-Varillas R, Lucchini M, and Nisoli M 2022 *Rep. Prog. Phys.* **85** 066401

[12] Zhao X, Li S, Driver T, Hoang V H, Le A T, Cryan J P, Marinelli A, and Lin C D 2022 *Phys. Rev. A* **105** 013111

[13] Wang J, Gao S N, Liu A, He L, and Zhao X 2025 *Sci. Rep.* **15** 117

[14] Nishitani J, West C W, Higashimura C, and Suzuki T 2017 *Chem. Phys. Lett.* **684** 397

[15] Nan Q W, Wang C, Yu X Y, Zhao X, Cheng Y, Gong M, Liu X J, Kimberg V, and Zhang S B 2023 *Chin. Phys. Lett.* **40** 093201

[16] Jiang L, Jiang C Y, Tian Y C, Zhao H, Zhang J, Tian Z Y, Fu S H, Liang E J, Wang X C, Jin C, and Zhao J 2024 *Chin. Phys. Lett.* **41** 047802

[17] Jin W, Wang C, Zhao X, Yang Y, Ren D, Liu Z, Li X, Luo S, and Ding D 2024 *Chin. Phys. Lett.* **41** 053101

[18] Shu Z, Liang H, Wang Y, Hu S, Chen S, Xu H, Ma R, Ding D, and Chen J 2022 *Phys. Rev. Lett.* **128** 183202

[19] Torres R, Kajumba N, Underwood J G *et al.* 2007 *Phys. Rev. Lett.* **98** 203007

[20] Vozzi C, Negro M, Calegari F, Sansone G, Nisoli M, De Silvestri S, and Stagira S 2011 *Nat. Phys.* **7** 822

[21] Yuan H, He L, Wang F, Wang B, Zhu X, Lan P, and Lu P 2018 *Opt. Lett.* **43** 931

[22] Chen Y J, Fu L B, and Liu J 2013 *Phys. Rev. Lett.* **111** 073902

[23] Hernández-García C, PicÓn A, San Román J, and Plaja L 2013 *Phys. Rev. Lett.* **111** 073902)

[24] Nourbakhsh Z, Tancogne-Dejean N, Merdji H, and Rubio A 2021 *Phys. Rev. Applied* **15** 014013

[25] Li X, Han J, Liu L, Wang X, Wang G, and Jin C 2024 *Phys. Rev. A* **109** 023103

[26] Zhou S S, Lan W D, Chen J G, Wang J, Guo F M, and Yang Y J 2022 *Phys. Rev. A* **106** 023510

[27] ao W, Wang L, Song P, Xiao F, Wang J, Zheng Z, Zhao J, Wang X, and Zhao Z 2023 *Chin. Phys. Lett.* **40** 063201

[28] Wang L, Wang X, Xiao F, Wang J, Tao W, Zhang D, and Zhao Z 2023 *Chin. Phys. Lett.* **40** 113201

[29] Zhang R, Wang F, Yuan H, Chen S, Yang C, Ou T, Song J, Liao Q, and Lu P 2024 *Phys. Rev. A* **109** 043118

[30] Fu T T, Guo F M, Zhou S S, Qiao Y, Wang X Y, Chen J G, Wang J, and Yang Y J 2023 *J. Chem. Phys.* **159** 164312

[31] Sun N, Zhu X, Wang B, Wang D, Shao R, Lan P, and Lu P 2020 *Phys. Rev. A* **101** 053437

[32] Qin M, Zhu X, Zhang Q, Hong W, and Lu P 2011 *Opt. Express* **19** 25084
[33] Zhao X, Wei H, Wu Y, and Lin C D 2017 *Phys. Rev. A* **95** 043407
[34] Le C T, Hoang V H, Tran L P, and Le V H 2018 *Phys. Rev. A* **97** 043405
[35] Kraus P M, Rupenyan A, and Wórner H J 2012 *Phys. Rev. Lett.* **109** 233903
[36] Phan N L, Le C T, Hoang V H, and Le V H 2019 *Phys. Chem. Chem. Phys.* **21** 24177
[37] Miao X Y and Du H N 2013 *Phys. Rev. A* **87** 053403
[38] Bian X B and Bandrauk A D 2011 *Phys. Rev. A* **83** 023414
[39] Zhang B, Chen Y, Jiang X, and Sun X 2013 *Phys. Rev. A* **88** 053428
[40] Xu L and He F 2019 *J. Opt. Soc. Am. B* **36** 840
[41] Li W Y, Yu S J, Wang S, and Chen Y J 2016 *Phys. Rev. A* **94** 053407
[42] Hu H, Li N, Liu P, Li R, and Xu Z 2017 *Phys. Rev. Lett.* **119** 173201
[43] Castro A, Appel H, Oliveira M, Rozzi C A, Andrade X, Lorenzen F, Marques M A, Gross E, and Rubio A 2006 *Phys. Status Solidi B* **243** 2465
[44] Andrade X, Strubbe D, De Giovannini U *et al.* 2015 *Phys. Chem. Chem. Phys.* **17** 31371
[45] Marques M A, Castro A, Bertsch G F, and Rubio A 2003 *Comput. Phys. Commun.* **151** 60
[46] Wardlow A and Dundas D 2016 *Phys. Rev. A* **93** 023428
[47] Klemke N, Tancogne-Dejean N, Rossi G M, Yang Y, Scheiba F, Mainz R E, Di Sciacca G, Rubio A, Kártner F X, and Múcke O D 2019 *Nat. Commun.* **10** 1319
[48] Tancogne-Dejean N, Múcke O D, Kártner F X, and Rubio A 2017 *Nat. Commun.* **8** 745